THE ASTRONOMICAL JOURNAL, 121:2392–2404, 2001 May
© 2001. The American Astronomical Society. All rights reserved. Printed in U.S.A.

QUASAR-GALAXY CORRELATIONS: A DETECTION OF MAGNIFICATION BIAS[1]

DARA J. NORMAN
Department of Physics and Astronomy, State University of New York at Stony Brook, Stony Brook, NY 11794-3800
AND
CHRIS D. IMPEY
Steward Observatory, University of Arizona, 933 North Cherry Avenue, Tucson, AZ 85721
Received 2000 December 21; accepted 2001 February 9

ABSTRACT

Weak gravitational lensing by clusters and superclusters can change our perception of the distribution of bright background quasars through the phenomenon of magnification bias. It has been suggested that this lensing will lead to an association of moderate-redshift quasars ($z \sim 1.0$–2.0) and foreground galaxies ($z \sim 0.2$–0.3). We report on the analysis of a sample of 90 CCD fields centered on moderate-redshift quasars that are bright at both radio ($S_{5\ \mathrm{GHz}} > 1$ Jy) and optical ($V < 21.0$) wavelengths, along with 12 control fields. The quasars presented here are chosen to have the highest potential for evidence of this weak lensing effect. We find no evidence for the presence of rich galaxy clusters (Abell richness class 1) in the foreground of these fields. However, using a Spearman rank-order correlation test, we detect a correlation between galaxy number density and angular distance from bright quasars on scales of $\sim 15'$ with a significance of 96%. The observed correlation is unlikely the result of Galactic dust and is consistent with weak gravitational lensing of the quasars by foreground matter. We also determine the two-point angular correlation function between these background quasars and foreground galaxies. We find a correlation amplitude of 0.056 ± 0.020 over scales of $\sim 5'$. This angular correlation is consistent with the semianalytic weak gravitational lensing models of Dolag & Bartelmann (published in 1997), which incorporate nonlinear evolution of mass clustering.

Key words: cosmology: observations — gravitational lensing — quasars: general

1. INTRODUCTION

Several studies have explored the association of foreground galaxies and moderate-redshift quasars. It is generally believed that this correlation is due to gravitational lensing (Canizares 1981; Schneider, Ehlers, & Falco 1992). Clusters of galaxies at redshifts of 0.2–0.3, near the quasar line of sight, are thought to trace the lensing mass required to magnify quasars at $z \sim 1.0$. As a result of this lensing effect, the brightest quasars will have an angular association with these concentrations of lower redshift galaxies. In particular, a magnification bias arises because gravitational lensing conserves surface brightness but changes the solid angle of the source. This change of solid angle means that a patch of sky behind a lens will have its dimensions stretched. An observer looking through a fixed aperture will then see a smaller region of sky than would have been observed in the absence of the lens. This will tend to dilute the number density of sources in the patch. However, because lensing will also magnify sources, intrinsically faint sources will be brightened into a flux-limited sample. Thus, the luminosity function of the source population has an important influence on the size of this magnification bias. Source populations with a steep luminosity function may show enhancements of the galaxy number density around these quasars, while populations with a more shallow slope will not show the enhancement or may even show a deficit.

Earlier studies have looked for quasar-galaxy correlations either in homogeneous samples on small scales of several arcseconds (Tyson 1986), or in inhomogeneous samples on scales of several arcminutes (see, e.g., Bartsch et al. 1997; Benítez & Martínez-González 1995, 1997) up to a degree (see, e.g., Williams & Irwin 1998; Norman & Williams 2000). These homogeneous observations on small scales have targeted only a few quasars. Because the magnification bias signal is weak, a large statistical sample of fields is needed to accurately determine the true amplitude of the signal. Theoretical predictions suggest that the scale of the correlations should be a few arcminutes. Previous studies of homogeneous samples do not allow us to test predictions on these scales.

Attempts to detect such a signal with inhomogeneous data are fraught with problems. Since these surveys have been done for a variety of different purposes, they are subject to a number of selection biases, making the weak signal of magnification bias difficult to accurately detect and measure. Bartelmann (1995, hereafter B95) discusses the criteria needed for a homogeneous survey of quasar fields sufficient enough to accurately determine both the amplitude and scale of the magnification bias of quasars due to weak lensing by foreground mass structures traced by galaxies. This determination of the shape, amplitude, and scale of the correlation can be used to set limits on cosmological parameters, as discussed later in this paper.

Here we have embarked on the survey similar to that outlined by B95. We have looked for galaxy excesses in fields centered on 90 radio-loud quasars. With this homogeneous sample of quasars and galaxies, we search for the signature of magnification bias on scales of up to $\sim 30'$. Section 2 is devoted to a description of the data used in the survey, while the galaxy sample is defined and examined in

[1] Based on observations obtained at the Kitt Peak National Observatory (KPNO) and the Cerro Tololo Inter-American Observatory (CTIO), a division of the National Optical Astronomy Observatories, which is operated by the Association of Universities for Research in Astronomy, Inc., under cooperative agreement with the National Science Foundation (NSF).

§§ 3 and 4. In § 5, we discuss tests used for measuring the galaxy overdensities, along with the possible effects of dust in our sample. Finally, we compare the results presented here with models of lensing in § 6.

2. OBSERVATIONS

As discussed in Norman & Impey (1999, hereafter Paper I), we have used quasar fields from the 1 Jy all-sky radio source catalog (Kühr et al. 1981). The catalog lists 527 radio sources with flux densities of $S_{5\ \mathrm{GHz}} \geq 1.0$ Jy and covers 9.81 sr of the sky at galactic latitudes of $|b| \geq \pm 10°$. Over 97% of the radio sources have also been optically identified (Stickel, Meisenheimer, & Kühr 1994). A total of 301 of these radio sources have been identified as quasars, and of these, 289 quasars have optical magnitudes of less than 21.0. The optical magnitudes of the quasars have been taken from the NASA/IPAC Extragalactic Database (NED). The magnitudes given are generally V-band magnitudes, often from different references using different optical setups. No attempt has been made to correct these various systems to a common scale, so this paper refers to optical magnitudes instead of V magnitudes in order to avoid confusion. In addition, radio-loud quasars are variable, so magnitudes listed in the NED are only roughly indicative of the average brightness. The only relevant issue for this paper is the preference given to optically bright quasars with a median magnitude of ~ 18.5, which guarantees quasars that are optically luminous.

During five observing runs at the KPNO Burrell Schmidt telescope and a single run at the CTIO 1.5 m Ritchey-Chrétien telescope, we observed 117 of these radio-bright quasars. We did not use 27 fields because of problems due to bad weather and/or with the guider. Figure 1 is a plot of radio fluxes for our final sample of 90 quasars versus their optical magnitudes.

We have imposed an optical magnitude cut of $R = 21.5$ in the hopes of taking advantage of the double magnification bias (Borgeest, von Linde, & Refsdal 1991).

To measure the signal of magnification bias, we are interested in the association of quasars with *foreground* galaxies, as opposed to galaxies associated with the quasar itself, therefore we have also restricted our quasar sample to have redshifts of $z > 0.7$ (see Fig. 2, in which we plot the number

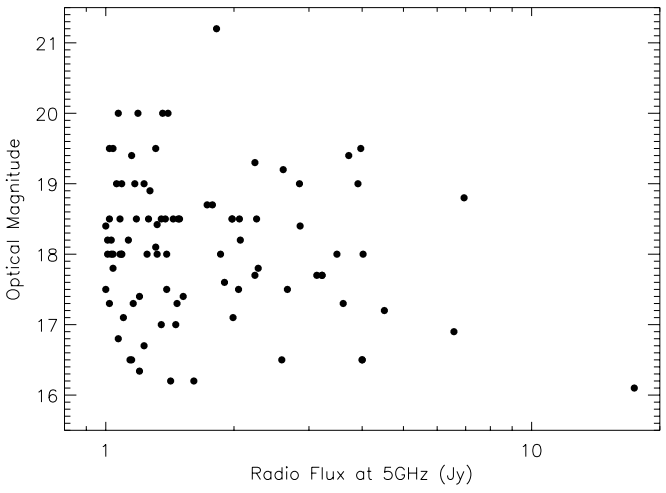


FIG. 1.—Plot of radio flux values vs. optical magnitudes for the 90 quasars imaged in this survey. The quasars are all from the 1 Jy catalog.

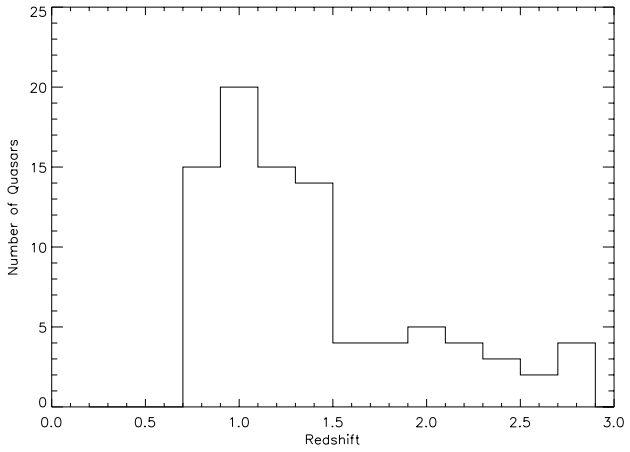


FIG. 2.—Histogram of the redshifts for the 90 quasars imaged in this survey. A redshift cutoff of $z > 0.7$ was imposed to limit contamination from galaxies physically associated with the quasars.

of quasars per redshift bin). This selection of redshift range is discussed further in § 5.

Of the 90 quasar fields used in this survey, 61 fields were observed with the Burrell Schmidt telescope at KPNO. The details of the observations and the reduction of the Schmidt data have been discussed in Paper I. For these large-format fields, star-galaxy separation must be done in a statistical sense. The method used to determine galaxy number density in these fields is outlined in Paper I as well; the reader is referred there for details.

The remaining 29 fields in the survey were observed with the Ritchey-Chrétien 1.5 m telescope during a single run in 1996 February at CTIO. The telescope has a 14.′7 × 14.′7 field of view and a 2048 × 2048 pixel Tek 2K CCD. This CCD is a mosaic of four detectors, each with its own readout array. This means that the bias and flat fields are different for each quarter of the image. The fields were sampled at 0.″432 pixel^{-1}. Images of the quasar fields are produced as a mosaic of a 3 × 3 grid of images with overlapping regions in order to increase our field size to ~ 40 arcmin^2, allowing us to look for quasar-galaxy correlations on scales of up to $\sim 15'$. Each of the nine pointings per field was observed with the Harris R filter and exposed for 360 s. Transparency for all nights was good, with a seeing of $\sim 1.''3$–$1.''4$. Landolt standard star (Landolt 1992) observations were taken on several occasions each night.

In addition, 12 "control" fields were observed at the Schmidt telescope. These fields have no bright quasars located in them. They have been analyzed in an identical manner to our program quasar fields, and they are described in more detail in Paper I.

3. DATA REDUCTION OF THE SOUTHERN FIELDS

Like the northern fields, these 29 fields were reduced with the IRAF processing package (Tody 1986). As mentioned above, the detector is a mosaic of four detector fields. The routine QUADPROC in the IRAF ARED package is specifically designed to apply the proper overscan regions and trim areas for each individual detector field. The four fields are then combined into a composite 14.7 × 14.7 arcmin^2 image. QUADPROC was first run on all the bias, flat, and program field frames to combine each into a single image field. The 15 bias fields taken at the start of each night were median combined and subtracted from the frames. We com-

bined all the flat fields taken during the six night run into a superflat field by scaling and averaging them. The bias-subtracted program fields were then flattened with this superflat. This procedure appears to do a good job of removing large-scale structure in the CCD frame, leaving a 1%–2% gradient across the sky in the frames.

The field of view of a single 1.5 m field is substantially smaller than the Schmidt field size of $1^\circ \times 1^\circ$, which was used for the northern quasars in the sample. In order to sample the area around the quasars on comparable angular sizes, we combined nine 1.5 m fields into a single mosaic of the region. The quasar is therefore centered on a 3×3 grid of 1.5 m fields. Bias-frame subtraction, flat-fielding, and object detection (discussed below) were done separately for each individual field. Fields were combined after matching objects in overlap regions of greater than 10% of the area.

Magnitudes determined for the common objects are seen to be in good agreement across different fields. The distribution has a full width of ~ 0.1 mag for objects with magnitudes brighter than 18.5, and ~ 0.25 for objects of fainter magnitude. Photometric errors for faint objects are not affected by any zero-point shifts associated with creating each mosaic.

Like the Schmidt fields, discussed in Paper I, we have used the FOCAS package to create object catalogs. Here too, we have limited the sky background range in the first row to insure that the detection of faint objects proceeds smoothly. Average sky background counts for the frames range from 350 to 1100 counts, so these fields are sky limited, as with the Schmidt data.

Optimal parameter settings for using FOCAS on these frames were determined empirically. A threshold of 2.5 σ above the background and a minimum total area of 10 pixels were chosen as the parameter settings. Because the sampling for these 1.5 m frames is $0''.432$ pixel^{-1}, stars and galaxies can easily be distinguished from cosmic rays, which cover only a pixel or two. The area threshold was initially chosen to be at least as large as the minimum area of a stellar image, given the average seeing over the six nights of $\sim 1''.4$. This minimum was later revised upward because of observations by eye and separation parameter plots that suggested that false detections could be more effectively eliminated with a larger area threshold of 40 pixels.

4. STAR AND GALAXY COUNTS

As compared with the Schmidt data in Paper I, the better sampling of the 1.5 m images allowed us to use a surface brightness method to separate stars from galaxies. The separation parameter is determined by comparing the core brightness of an object (central 3×3 pixels) with the total brightness of that object. For stars, this parameter is independent of magnitude. The stellar locus is apparent in the field, although it differs from field to field because of seeing differences and crowding. Figure 3 shows the separation parameter (core magnitude minus total magnitude) for the field around quasar 0858−279 plotted against total magnitude. This field is typical of all the 1.5 m data.

Each of the nine fields has been adjusted in the plot so that the stellar loci match. The stellar locus is clearly visible in each field. However, each quasar field image is a little different, with some fields showing clearer separations between stars and galaxies because of variable seeing within the regions that make up a mosaic and/or crowding. In nearly every case, the method breaks down below R magnitudes of ~ 20–20.5. The 1.5 m galaxy sample has been defined as those objects with separation parameters lying above the stellar locus at magnitudes brighter than 21.0. The last magnitude bin in Figure 4 shows that with these criteria, we are likely incomplete at $R = 20.5$–21. In the analysis that follows, we also look at the stellar sample, chosen to be those objects at magnitudes brighter than 21.0 with separation parameters lying below the upper edge of the stellar locus; again, this edge will vary from field to field.

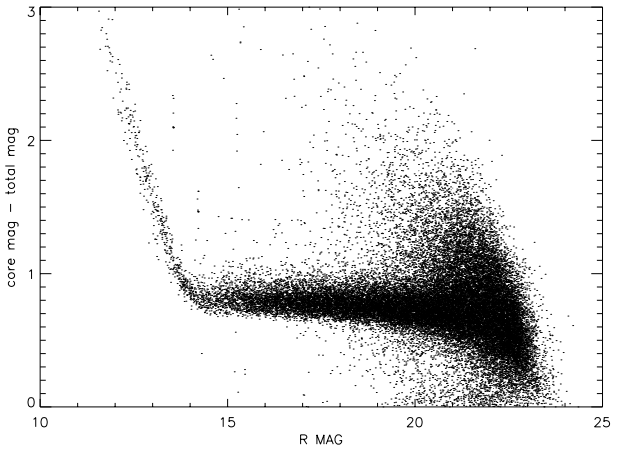


FIG. 3.—Representative plot of the total magnitude vs. separation parameter for the sample 1.5 m fields. The field shown is 0858−279. All objects detected in the mosaic of the nine pointings in each field are plotted and scaled so that the stellar loci match.

Many of the southern quasar fields are located at fairly low galactic latitudes ($10 < |b| < 20$). At these low galactic latitudes, many more stars are expected in the fields as the field latitude approaches the galactic plane. In Figure 5, we plot the number of stars per square degree in the magnitude range $R = 19.5$–21.0 as filled circles, and the number counts from Metcalfe et al. (1991, hereafter MSFJ) as asterisks. The plot shows the expected steep rise in star counts for fields located closer to the galactic plane, with a rise by an order of magnitude from 45° to 10°. These findings are quite consistent with those of MSFJ, in which they too find an increase of stars toward lower latitudes. However, we

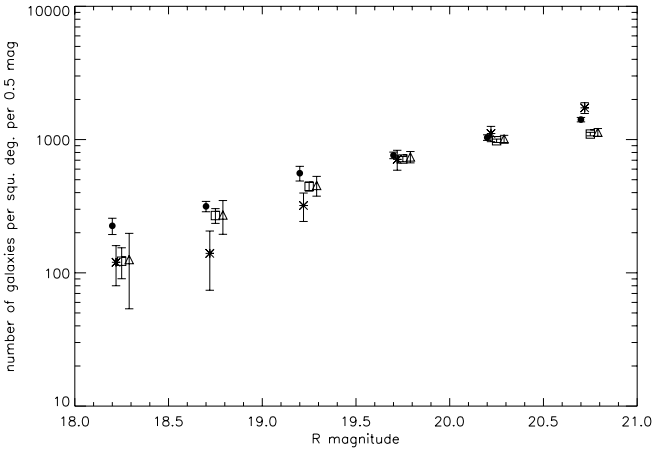


FIG. 4.—Number of galaxies per square degree per 0.5 mag interval plotted vs. field galactic latitude. Squares show the Schmidt quasar fields, triangles show the Schmidt control fields, filled circles show the 1.5 m fields, and asterisks show Metcalfe et al. (1991) fields. Errors plotted are $N^{1/2}$ variation in the number of galaxies per field.

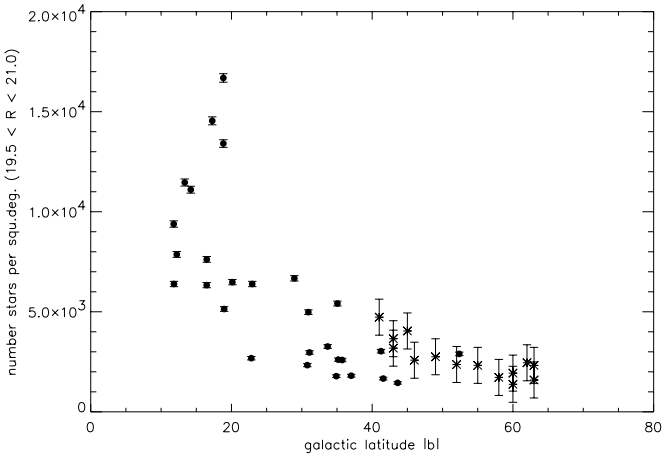


FIG. 5.—Number of stars per square degree in a $19.5 < R < 21.0$ mag interval plotted vs. field galactic latitude. The 1.5 m fields are plotted as filled circles, and Metcalfe et al. (1991) fields are plotted as asterisks. Errors plotted are $N^{1/2}$ variation in the number of stars per field.

should expect no such trend with latitude in our galactic sample, if the sample is indeed free of stellar contamination. Figure 6 includes the number of galaxies per square degree in the magnitude range $R = 19.5$–21.0 for the 1.5 m data, plotted as filled circles. This plot shows no trend of the data

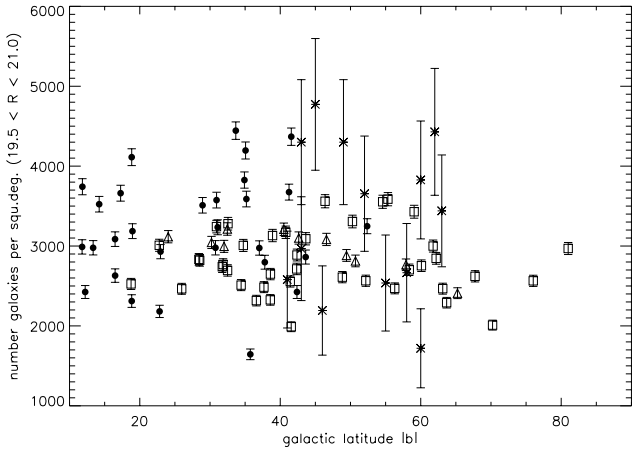


FIG. 6.—Comparison of the number of galaxies per square degree in the magnitude interval $19.5 < R < 21.0$. Squares show the Schmidt quasar fields, triangles show the Schmidt control fields, filled circles show the 1.5 m fields, and asterisks show MSFJ fields. The rms errors are also plotted.

with latitude, even to the lower latitudes of 10°, indicating that our galaxy counts are statistically unbiased by stellar contamination. The scale of the number of galaxies also agrees well with those found in the Schmidt fields (*squares*) and those of MSFJ (*asterisks*).

We would also like to compare the galaxy fractions found in the 1.5 m frames with those found by MSFJ and in our 90 inch (2.3 m) Schmidt overlap comparison frames (described in Paper I). However, from Figure 5, one can see that the low-latitude frames will be overwhelmingly dominated by stellar counts. We therefore compare the galaxy fractions found on the 1.5 m frames only for those fields that are at the higher galactic latitudes. Table 1 lists the galaxy and star number counts for MSFJ and our galaxy counts for both the 1.5 m fields and 90 inch comparison fields. Column (1) gives the R-magnitude ranges. The number counts of galaxies and stars per square degree, along with the fraction of galaxies listed in Table 5 of MSFJ, are reproduced here in columns (2)–(4). Column (5) gives the galaxy fraction for the comparison 90 inch fields, as discussed in detail in Paper I. The final columns of Table 1 list the galaxy fractions determined from the 1.5 m fields. In column (6), we show the galaxy fractions for all fields with $|b| > 25°$. Three of these fields have slightly higher numbers of stars for their galactic latitude, although they are not out of range of the projected MSFJ star counts for low latitudes. If these fields of high-stellar densities are eliminated, then the galaxy fractions are those listed in column (7). These galaxy fractions obtained for the 1.5 m fields are slightly lower than those measured for the 90 inch or MSFJ fields. It appears that this can be attributed to the range of galactic latitudes of the majority of the 1.5 m fields. While all the MSFJ fields and most of our Schmidt fields lie at latitudes higher than $\pm 40°$, most of the 1.5 m fields have $|b| < 40°$. Thus, they are expected to be more heavily contaminated with stars. However, the agreement of the inferred number of galaxies per square degree of these fields with both the MSFJ and Schmidt counts (Fig. 4) suggests that we have adequately accounted for the offending stars with the surface brightness separation method.

Having demonstrated that our 1.5 m galaxy sample can be adequately corrected for stellar contamination, we now wish to compare the number counts of the galaxies with those obtained from the Schmidt fields and also from other galaxy surveys. In Figure 6, we have overplotted the average number of galaxies per square degree in the magnitude range 19.5–21.0 as a function of galactic latitude (*filled circles*). These 1.5 m galaxy counts are in excellent agreement with the number counts obtain previously for the

TABLE 1

GALAXY AND STAR COUNTS

R mag (1)	MSFJ No. of Galaxies (per deg^2) (2)	MSFJ No. of Stars (per deg^2) (3)	Galaxy Fractions (4)	Galaxy Fractions (90 inch) (5)	Galaxy Fractions (1.5 m, $\|b\| > 25°$) (6)	Galaxy Fractions (1.5 m, low stars) (7)
18.0–18.5...	120	375	0.24	0.24 ± 0.28	0.24	0.28
18.5–19.0...	140	200	0.41	0.30 ± 0.37	0.30	0.34
19.0–19.5...	320	300	0.52	0.52 ± 0.34	0.38	0.43
19.5–20.0...	710	375	0.65	0.62 ± 0.38	0.45	0.49
20.0–20.5...	1110	425	0.72	0.64 ± 0.16	0.50	0.54
20.5–21.0...	1730	625	0.72	0.72 ± 0.11	0.54	0.59

NOTE.—MSFJ: Metcalfe et al. 1991.

Schmidt fields. We conclude that, like the Schmidt sample, our 1.5 m galaxy sample can be successfully corrected for stellar contamination and is quite consistent with R galaxy counts obtained from other surveys. Equivalently, the 1.5 m sample corroborates our assertion in Paper I that the Schmidt galaxy sample is statistically reliable.

In practice, we wish to combine our 1.5 m galaxy survey with our Schmidt survey in order to increase the size of our statistical sample of quasar fields. For the Schmidt galaxy sample, we were required to limit the magnitude range of galaxies to $R = 19.5$–21.0 in order to avoid excessive stellar contamination of the sample. The surface brightness method used for the southern fields is capable of distinguishing stars from galaxies at brighter magnitudes; however, to maintain the homogeneity of the combined sample, we also limit the magnitude range of the southern galaxy sample to $R = 19.5$–21.0.

5. THE DETECTION OF EXCESS GALAXIES NEAR QUASARS

With this survey, we are looking for a signature of magnification bias in this sample of bright radio quasars. We expect this to be detected as an excess of galaxies in a circular region around these quasars, as compared with the ambient background number density of galaxies on the sky. The agreement with published galaxy number counts shown in Figure 4 indicates that we have accounted for contaminants like stars, cosmic rays, and potential false detections from our galaxy sample. An accurate accounting of these contaminants is particularly important for our ability to measure an excess near our quasar because each of these contaminants is uncorrelated with the quasar position and will dilute the anticipated correlation signal.

The magnitude range of the galaxies in the survey has been chosen to exclude galaxies that are physically associated with the quasars. As shown in Figure 2, the quasar sample contains only quasars with $z > 0.7$. Therefore, the galaxy sample has been chosen in such a way that nearly all the galaxies used in this survey are at magnitudes too bright to be at the quasar redshifts. The Automatic Plate Measuring Facility (APM) survey (Maddox, Efstathiou, & Sutherland 1996) and other deep surveys (see, e.g., Broadhurst, Ellis, & Shanks 1988; Colless et al. 1993) have found that galaxies with red magnitudes similar to those in this sample have redshift distributions that peak well below $z = 1.0$. For the APM survey, the redshift distribution of blue galaxies with magnitudes of $B \sim 17$–21, converted from the APM b_j system, peaks at a redshift of about 0.2, with few galaxies beyond $z = 0.7$ (Maddox et al. 1996). These blue magnitudes correspond to our R-magnitude range, if we assume a color transformation of $B - R = 1.5$, as found by Williams & Irwin (1998) for field galaxies from the APM survey in the magnitude range $18.5 < R < 20.0$.

Similarly, Broadhurst et al. (1988) find for galaxies with $b_j = 20.0$–21.5 ($R \sim 19$–20.5 for elliptical galaxies) that the number distribution as a function of redshift peaks at $z \sim 0.2$, with none of their galaxies beyond a redshift of 0.7. Thus, the galaxies detected in this survey are likely to be at much lower redshifts than the quasars. Consequently, any measured angular correlation of the galaxies with the quasars is not due to physical proximity.

5.1. *Number Excess*

As an initial test of galaxy overdensity in the vicinity of quasars, each field was divided into two regions; an inner region that encompassed 50 arcmin^2 around the quasar position and an outer background region that, because of the field sizes of the two telescopes, is necessarily different for the northern and southern data sets. The inner region is a circular area centered at the position of the quasar, with a radius of 4′. This radius corresponds to about 0.6–0.8 h_{100}^{-1} Mpc at the most probable redshift of lensing galaxies, $z = 0.2$–0.3. This is about twice the core radius of a rich galaxy cluster.

5.1.1. *Northern Fields*

For the Schmidt fields, an annulus from 15′ to 25.′0 was used to determine the galaxy background, or the mean number of galaxies on a randomly chosen piece of the sky. The inner value of the background radius was chosen to be outside the predicted scale of the angular correlation from semianalytic models of the magnification bias (B95; Sanz, Martínez-González, & Benítez 1997; Dolag & Bartelmann 1997, hereafter DB97). The outer background radius is defined by the perimeter of each CCD frame. We count the number of galaxies in each annular region with magnitudes of $R = 19.5$–21.0. The scaled average number of galaxies for a 50 arcmin^2 background region is 39, with an rms scatter of about 20% between the fields.

The excess number of galaxies in each field is defined as the number of galaxies in the center 50 arcmin^2 minus the scaled average number of galaxies in a 50 arcmin^2 background region. Figure 7 shows a histogram of the number of fields with a given excess, with control fields plotted as dotted lines. The average galaxy excess for the quasar fields is 3.0 ± 7.4. This is consistent with no average excess, and the distribution shows very few large enhancements of galaxies near the quasar position.

5.1.2. *Southern Fields*

A similar test has been performed on the 1.5 m fields. However, because of the smaller area of sky covered in these mosaics, the background region is restricted to annuli at radii of 10.′5–15.′0 from the central quasar position. Here too, the central area is a 4′ radial region (50 arcmin^2) around the quasar position. The average number of back-

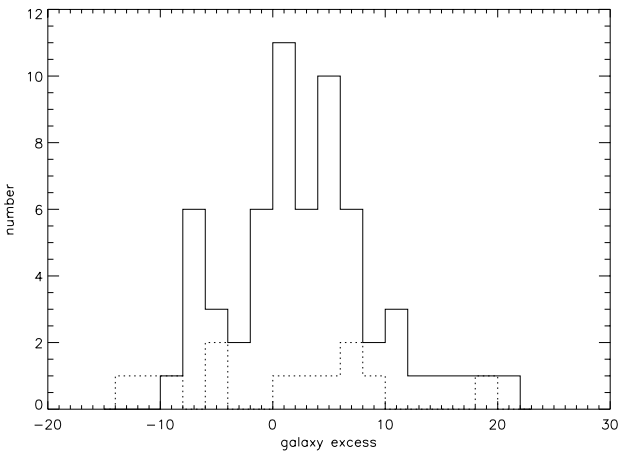


FIG. 7.—Histogram of the galaxy excess for the Schmidt fields. The solid line shows the histogram for the quasar fields, while the dotted line shows the histogram for the control fields. The galaxy excess is defined as the difference between the number of $R = 19.5$–21.0 galaxies in a central 50 arcmin^2 area around the quasar of radius 4′ minus the scaled number of galaxies in a background region extending from 15′ to 25′.

ground galaxies per 50 arcmin^2 for these 1.5 m fields at 45 ± 10 galaxies, in statistical agreement with our Schmidt counts. Like the Schmidt fields, the galaxy excess shows no trend with galactic latitude. As with the Schmidt fields, a histogram of galaxy excess (Fig. 8*a*) shows a distribution without large galaxy excesses in the central region. For these fields, the distribution average is 1.4 ± 12.6, consistent with no central excess, on average.

Because galaxies and stars have been separated in these 1.5 m fields via a surface brightness test, it *is* known which objects in these fields are stars and which are galaxies. In the absence of significant galactic dust problems, galactic star positions should show no correlation with the quasar positions in these fields. Therefore, a plot of the excess numbers of stars in the central region versus the background area should show no significant excess. Gross problems in these fields caused by the CCD, dust, etc., could then be eliminated by measuring any such stellar correlations. No variation in the stellar number density is seen across each field. The rather large variation of stellar number density over the magnitude range $19.5 < R < 21.0$ between these fields (from ~ 25 to 225) appears to be real galactic variation. This is not surprising given that the range of galactic fields here is from 11° to 53° (also see Fig. 5). However, there is no trend in the excess numbers of stars with galactic latitude as expected, since the stars, regardless of latitude, should know nothing of the quasar location. The distribution of stellar excesses in the central region of these 1.5 m fields (Fig. 8*b*) is not significantly different from the measured galactic excess distribution. This is confirmed with a Kolmorogov-Smirnov test. Both distributions are consistent with a mean of zero indicating no average excess.

A simple method has been exploited here to search for an excess of galaxies with $R = 19.5$–21.0 in the fields around 90 quasars. This measurement of the excess number of galaxy counts is done by comparing the number of galaxies in a 50 arcmin^2 region, centered at the quasar, with an average background density. We find that all the fields (northern and southern) show good agreement with a background density of about 40 galaxies in a 50 arcmin^2 region. We find only three fields that show a central excess of larger than 20 galaxies in either the northern or southern samples. The excess galaxy distributions in both samples are approximately Gaussian and statistically consistent with a mean of zero. In addition, we have performed other control experiments in which one expects to see no significant galaxy excess. For the northern fields, we looked at off-center excess (i.e., the inner region is not centered on the quasar location) measurements (see Paper I for further details), and for the southern fields, we looked at radial star distributions. Both tests lead to null results: there is no measurable difference between the distributions where no excess is expected and those in which a detection of excess is being sought. Thus, we find no significant excess of galaxies around the positions of the 90 quasars.

As a different kind of test, we also checked to see whether we could have detected an excess due to a cluster at $z = 0.2$–0.3, located in the foreground of one of these quasars, with the above method. We used as an example the X-ray cluster Abell 2390 (richness class 1), which has been examined extensively by Abraham et al. (1996). Abell 2390 spans a redshift range of 0.2–0.265. The limiting magnitude of the photometric survey of this cluster is $r_{\rm gunn} = 23.4$–24, with a color completeness of $r_{\rm gunn} = 21.0$. Although we have no color information for our galaxies, we can approximately convert our R magnitudes to $r_{\rm gunn}$ magnitudes, following MSFJ, with $R = r_{\rm gunn} - 0.3$.

From Abraham et al. (1996), we count 39 cluster member galaxies in a 4′ radial region from the cluster center, with magnitudes $19.8 < r_{\rm gunn} < 21.3$. The average number of galaxies we would predict from background counts in our outer annulus is ~ 40. Therefore, a total of ~ 80 galaxies is expected in a 4′ radial region, if a cluster as rich as Abell 2390 were in the foreground. Figures 7 and 8*a* show that only three fields in total show excesses on the order of 20 galaxies or more. An excess of 40 galaxies in any of these fields would be 4–5 σ above the mean background and clearly detectable. We therefore exclude the presence of such galaxy clusters along the lines of sight to *any* of these quasars. The presence of clusters 3–4 times less populated is also ruled out in the majority of these quasar sight lines.

However, as pointed out by B95, Bartelmann & Schneider (1991), Wu & Fang (1996), and others, it is possible that larger scale, lower contrast structures are present along these quasar sight lines. Detection of such structure with the excess method used above may be overwhelmed by cosmic

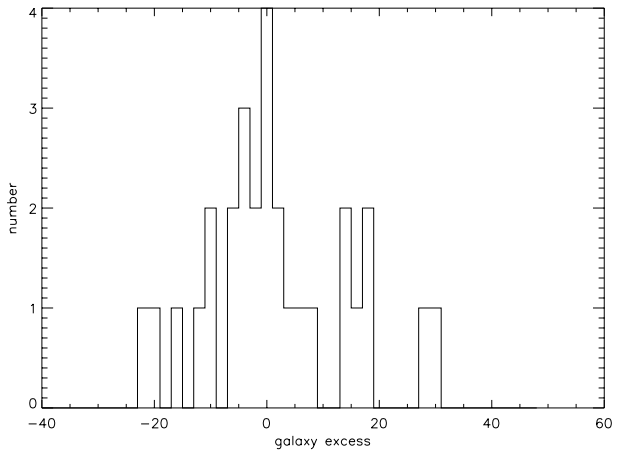


Fig. 8*a*

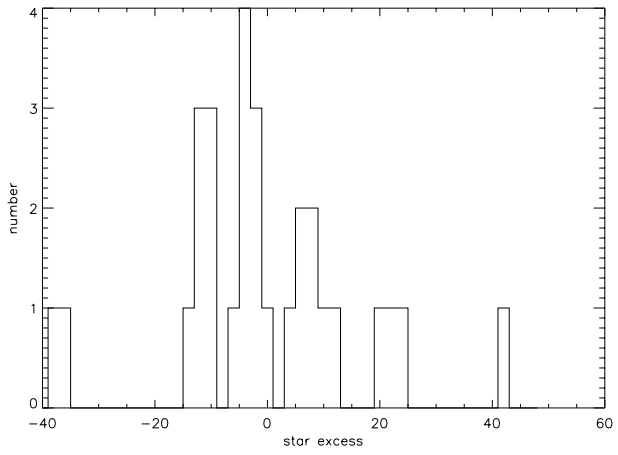


Fig. 8*b*

FIG. 8.—Histogram of the (*a*) galaxy and (*b*) star excesses for the 1.5 m fields. The galaxy and star excesses are defined in a similar way as in Fig. 9; however, the background region here extends from 10′.5 to 15′.0.

variation among the fields and the unknown shape of the lensing structures. We therefore employ a second statistical method to search for such large-scale structures.

5.1.3. *Rank-Order Correlations*

From the previous analysis, it is clear that if there is any overdensity in the number density of galaxies in these fields, its presence is subtle. Perhaps the structures we are seeking to identify have much lower number density contrast than Abell richness class 1 clusters. A second statistic is employed below to sensitively look for overdensities in these fields. Following Bartelmann & Schneider (1993a, 1993b, 1994), a Spearman rank-order correlation test (Press et al. 1986) is used to detect any gradient in the galaxy density with distance from the quasar. This nonparametric test is sensitive to any form of radial gradient across a single field. The data are replaced by a series of rankings, thus the results are invariant under any monotonic transformations. Replacement with rankings also tends to reduce the influence of outliers on the results. The mathematical details of this method are outlined in Paper I and therefore are not repeated here. However, the procedure can be summarized as follows: The individual fields are stacked on the positions of the central quasar. To apply this method, we have coadded the Schmidt and 1.5 m fields separately because of the different angular sizes of the fields. For each Schmidt or 1.5 m quasar field, 39 or 14 annuli of approximately equal areas (50 arcmin^2) are defined, centered on the position of the quasar. These 50 arcmin^2 annuli were chosen in order to have sufficient galaxies per region for good counting statistics, yet small enough that more than 10 annuli could fit across our CCD frames. At least 10 regions are necessary for the rank-order statistic to produce reliable results (Kendall & Stuart 1973).

The actual usable area of any particular field may be slightly less than 50 arcmin^2 because of bad regions on the chip. These areas are corrected for in each field prior to creation of the "superfield" and they amount to less than 2% of any given field. The superfield is created by summing all the galaxies in any given annulus over the 61 or 29 quasar fields. The rank-order correlation coefficient (r_c) is computed separately for the Schmidt and 1.5 m superfields. As usual, the higher the correlation coefficient, the more significant the correlation (see Paper I for details).

Table 2 below shows rank-order results for the 61 Schmidt quasars and 12 Schmidt control fields, as well as for the 29 1.5 m fields. The correlation coefficients and the corresponding error probabilities are listed for the field samples. For galaxies with $19.5 < R < 21.0$ in the quasar-centered Schmidt fields, we do find a correlation ($r_c = +0.28$) with a 96% significance. Neither the bright quasar-less control fields nor the off-center fields show any correlation.

TABLE 2

RANK-ORDER TEST FOR QUASAR-GALAXY ASSOCIATION

Field Type	r_c	ϵ
Schmidt quasar (on center)	+0.28	0.04
Schmidt quasar (off center)	−0.20	0.88
Schmidt control (on center).....	−0.23	0.91
Schmidt control (off center).....	−0.50	0.51
Schmidt stars (on center).....	+0.01	0.47
1.5 m galaxies ($R > 19.5$).....	+0.29	0.16
1.5 m stars ($R > 19.5$)	−0.42	0.93
1.5 m galaxies ($R > 15.0$).....	+0.48	0.04
1.5 m stars ($R > 15.0$)	−0.14	0.68

NOTE.—r_c is the correlation coefficient and $\epsilon = 1 =$ significance.

We might expect that this rank-order test would do a better job of distinguishing our on- and off-center fields than the initial test because it is more sensitive to gradients from the central point on any scale up to the half-angular width of the CCD frame. For the off-center analysis, any gradients over the concentric annuli would be washed out by the sampling. These results indicate that there does appear to be a marginally significant increase in the number density of galaxies closer to the positions of bright radio quasars.

Stars in these fields should not show any significant gradient with respect to the quasar positions. Although the Schmidt field stars cannot be individually separated from galaxies, we can select a magnitude range such that stars (and not galaxies) dominate the numbers of objects in the sample. Listed in Table 2 (as "Schmidt stars") is the correlation coefficient for objects in the Schmidt fields with $12.0 < R < 18.0$. For this sample of objects, which is assumed to be mostly made up of stars, $r_c = +0.01$, indicating no correlation.

The plot in Figure 9*a* shows the number of galaxies for the composite of 61 Schmidt fields with magnitudes of $R = 19.5 - 21.0$ in each annulus. This graph shows that there are not a few bins that dominate the correlation, but that there is indeed an overall trend of decreasing number density the farther the annuli are located from the quasar. The vertical errors are the 1 σ deviations of the number densities in each annulus and the horizontal lines indicate the width of the annulus. Each annulus has an area of 50 arcmin^2. Figure 9*b* shows a similar plot for the 12 control fields, with the number density scaled to compare with the quasar-centered fields, since fewer control fields are used. This plot shows no trend of number density of galaxies with distance from the "central" position. There is, however, a slight increase in the average number density for these control fields as compared with the quasar fields. This is likely statistical fluctuation because of the small number of control fields in this sample.

The galaxies from the 1.5 m sample show only a very slight gradient ($r_c = +0.29$, $\epsilon = 0.16$)[2] with position from the quasar, while the stars in these fields ($19.5 < R < 21.0$) show a slight anticorrelation ($r_c = -0.41$, $\epsilon = 0.93$). For the Schmidt fields, the galaxy sample must be limited to objects with $19.5 < R < 21.0$ because we are unable to individually eliminate stars, and because it must be in a magnitude region where stellar contamination can be considered negligible. However, no such restriction is required for the 1.5 m fields because a surface brightness test was used to segregate stars and galaxies, allowing this sample to be extended to brighter magnitudes to improve the statistics. An extension of the sample to magnitudes of $R = 15.0$ adds few galaxies, but the correlation with quasar position does become

[2] Note that although the correlation coefficients are of similar values for the Schmidt and 1.5 m quasar fields, the difference in the degrees of freedom, N, that is, the number of annuli used in the ranking, changes the significance of the value of r_c. The 1.5 m fields have only 14 annuli, so for the same value of r_c, the significance is less than for the Schmidt fields.

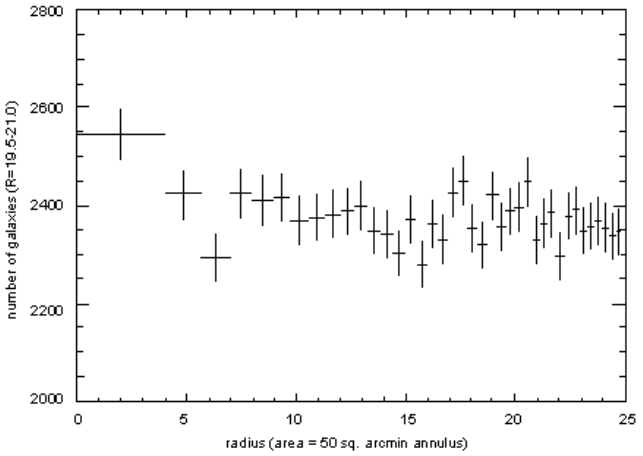


Fig. 9*a*

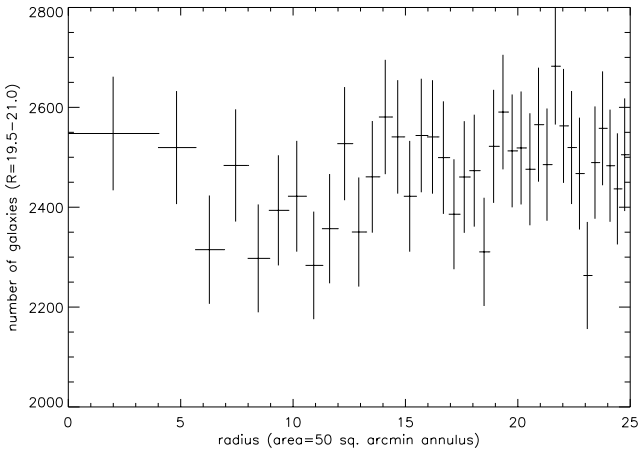


Fig. 9*b*

FIG. 9.—(*a*) Number of galaxies with magnitudes of $19.5 < R < 21.0$ vs. radius for the 61 stacked Schmidt quasar fields. (*b*) Number of galaxies vs. radius for the 12 Schmidt control fields. The horizontal error bars designate radial bins with an equal area of 50 arcmin^2. Vertical error bars are $N^{1/2}$. A gradient is detected for the quasar fields but not for the control fields with a rank-order analysis (see Table 2).

stronger (and more significant) for the galaxies with $r_c = +0.48$ with a 96% significance. Correspondingly, the extension of the stellar magnitude to $R = 15.0$ gives a correlation coefficient of -0.14, consistent with no correlation (see Figs. 10*a* and 10*b*).

The creation of a "superfield" by stacking the fields at the position of the quasars enables us to reduce cosmic variations in galaxy count between the fields. Figures 9*a* and 10*a* show that there is an enhancement in the number density of galaxies in angular regions closer to the quasar position in both data sets. This enhancement is confirmed by the rank-order analysis and is not seen in the control fields or in the samples dominated by stars.

5.2. *Angular Correlation Function*

Here we investigate the gradient detected through rank-order analysis in more detail by determining the angular quasar-galaxy correlation, $\omega_{QG}(\theta)$, as a function of θ, the angular separation from the quasar. With an estimate of the redshifts of the galaxies in the sample, the angular extent of this correlation can be translated into a physical size of hypothetical lensing structures.

In the analysis that follows, the northern and southern data sets have been combined, and we use only galaxies in the magnitude range $19.5 < R < 21.0$. Clearly, combining the two sets will increase our ability to measure this statistical correlation, as well as reduce the errors in the determination of the magnification bias signal. However, as noted earlier, the 1.5 m data have a field size smaller than that of the Schmidt fields. In combining the two data sets, the angular extent investigated must be trimmed to scales of less than 15′. In Figure 9*a*, it appears that the overdensity seen in the Schmidt fields is confined to small scales, that is, angular regions less than 10′ and probably even less than 6′. With no evidence of overdensities on scales larger than 15′, we conclude that little is lost in measuring the shape and scale of the correlation by the truncation of the Schmidt fields.

In the analysis that follows, the sampling of the data is changed slightly. In the previous analysis, the annular

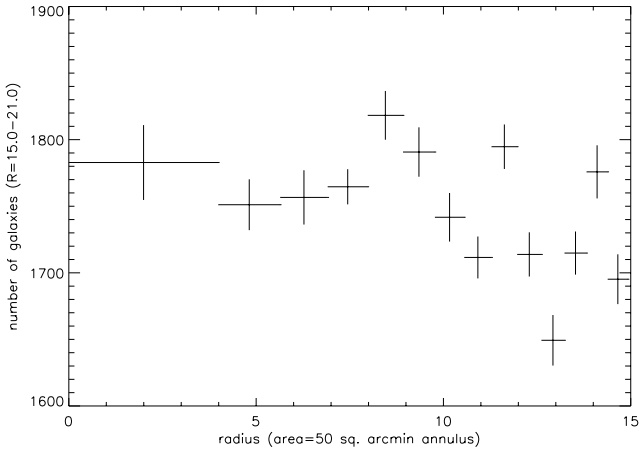


Fig. 10*a*

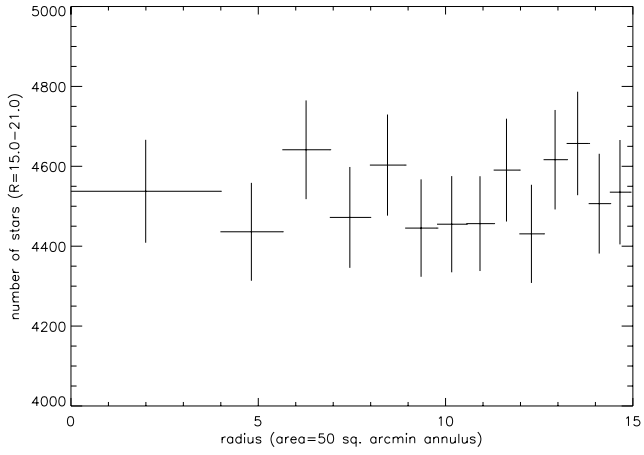


Fig. 10*b*

FIG. 10.—(*a*) Number of galaxies with magnitudes of $15.0 < R < 21.0$ vs. radius for the 29 stacked 1.5 m fields. A gradient is detected here with a rank-order analysis. (*b*) Number of stars in the same magnitude range vs. radius for the 1.5 m fields. The error bars are as in Fig. 11.

regions were split into regions of equal area, enabling a fair comparison of the galaxy number density. With a rank-order analysis, it is important to have regions of about the same area and thus similar statistics among the annuli. For the two point correlation analysis, we adopt outer annuli with constant widths of 0.75, along with a central annulus with a radius of 5.2, to improve the counting statistics. Otherwise, the central area is too small for good statistical sampling. Annuli with different areas are easily accounted for in the method used to determine the angular correlation described below.

The two-point correlation function provides a general purpose measure of the clustering of objects, based not on physical clustering, but on an association that has variable power on different angular scales. Thus, the angular correlation function has often been used (Tyson 1986; Benítez & Martínez-González 1995; and others) to determine the strength and scale of correlations of foreground galaxies in the fields of quasars. The estimator used here to compute the quasar-galaxy correlation function is defined by the function

$$\omega_{\rm QG}(\theta) = \frac{D_Q D_G}{\langle R_Q D_G \rangle} - 1 \ . \qquad (1)$$

Here, $D_Q D_G$ is the number of quasar-galaxy pairs within a given angular separation θ, and $R_Q D_G$ is the number of random quasar-galaxy pairs. In each of these fields, there is only one bright radio quasar, so the number of quasar-galaxy pairs is equal to the number of galaxies. The numerator is computed in a similar way to the previous overdensity analysis (with the new sampling described above); that is, annuli are centered at the position of the quasar, and the numbers of galaxies in each annulus are counted.

The quantity R_Q is determined by randomly "scattering" the central quasar position. The scattering is done such that the outer annuli around the fake quasar positions do not significantly occult the edge of the CCD. For each of the 90 quasar fields, 100 randomized quasar positions are created and numbers of galaxies are counted in each annulus out to $\sim 15'$. The average of these 100 experiments is then is used as the denominator in equation (1). Initially, $\omega_{\rm QG}(\theta)$ is computed for each of the 90 quasar fields. Figure 11*a* shows the average of these individual correlation functions. The errors shown are 1 σ rms errors in the mean for the 90 quasar fields. The same method has been used to determine $\omega_{\rm QG}(\theta)$ for the 12 control fields. This function is plotted in Figure 11*b*. These fields show no trend with angular scale, although the errors are large.

As expected, $\omega_{\rm QG}(\theta)$ has a mean of zero with small scatter in the background regions ($\theta = 6'$–$15'$). The correlation signal at positions close to the quasar is small and only marginally detected. The amplitude of the correlation for $\theta < 5.2$ is 0.056 ± 0.020: this signal is compared with other observational works later in the paper.

As seen in our earlier analysis, there is a correlation signal on a scale of $\lesssim 5'$. If a redshift is assumed for the lensing structures, then this angular scale ($5'$) can be translated into a physical size of the lens. In earlier sections, we argued that galaxies used in this survey must be located primarily at redshifts of $z = 0.2$–0.3 because of their magnitude range ($19.5 < R < 21.0$). At these distances, an angle of $5'$ corresponds to a physical size of 0.8–1.0 h_{100}^{-1} Mpc.

5.3. *Lensing versus Dust*

The issue of dust has also been discussed by various authors as a possible explanation for the observed angular correlations between quasars and galaxies. The quasars selected for this survey are all radio-bright and hence should be less affected by dust; however, here the possibility of dust as an explanation for correlations in this sample must be entertained. Since a galaxy overdensity (in contrast to an underdensity) is observed here, if dust plays an important role, it is expected that local galactic extinction is the primary cause.

In order to quantify the amount of galactic dust in these quasar fields, we look to the maps of Schlegel, Finkbeiner, & Davis (1998). These dust maps are calculated from 100 μm observations by the *COBE* DIRBE and *IRAS* ISSA missions, which cover the full sky at a resolution of $\sim 0.^\circ 7$. For the positions of each of the 90 quasars, the $E(B-V)$ color excess values are plotted in Figure 12 against the galactic latitude of the field. As expected, there is a strong

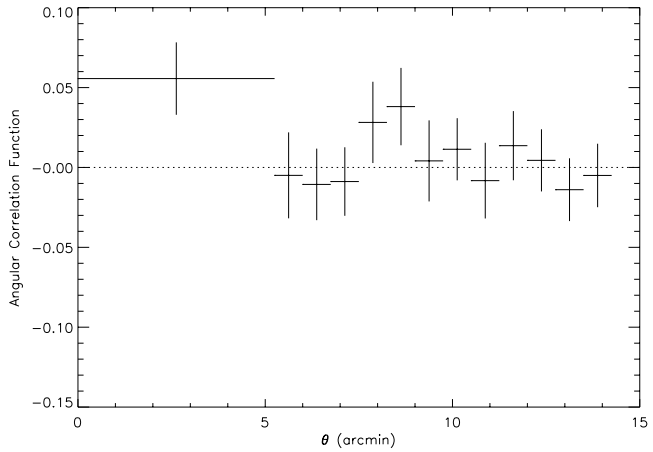


Fig. 11*a*

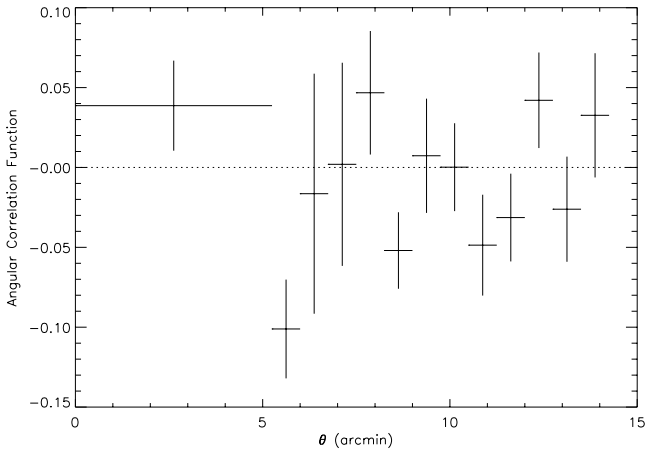


Fig. 11*b*

FIG. 11.—(*a*) Quasar-galaxy angular correlation function for the 90 fields in this survey. The plot shows an enhancement in the number of galaxies at angular positions near the quasar for $\theta < 5'$. The horizontal bars show the width of the annuli over which the galaxy count is binned. The vertical bars are 1 σ rms errors between the 90 individual fields. (*b*) Same plot as in (*a*), but for the 12 Schmidt control fields.

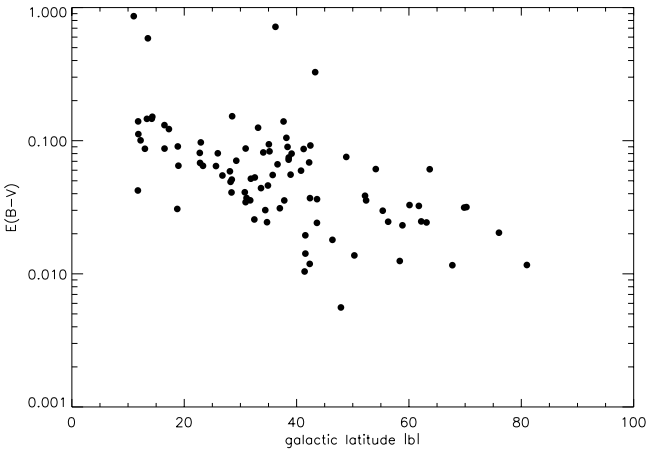


FIG. 12.—Color excess in the line of sight to each quasar, $E(B-V)$, vs. the galactic latitude of the quasar. The $E(B-V)$ values are obtained from maps by Schlegel et al. (1998). As expected, there is a strong trend of the color excess with distance from the galactic plane. Four fields show substantially more reddening than the other 86 fields.

correlation between increasing extinction and lower galactic latitude. Nearly all the color excess values fall between 0.05 and 0.2; however, there are four fields that have significantly larger extinction than the other fields. Plots of $E(B-V)$ against the optical magnitudes and radio fluxes of the quasars show no correlations. This suggests that the apparent brightnesses of these quasars are not affected by large amounts of galactic dust.

A comparison of the correlation function without these four high-extinction fields shows that the amplitude of the central bin is still 0.056 ± 0.020. Another method of testing whether the observed correlations are due to lensing effects or to dust is to look at the signal in subsamples of quasars. In particular, if the correlations are due to dust, then as the redshift distribution of the sources shifts to higher redshifts, the correlation strength should not change. This is because an observed overdensity due to dust must be caused by local Galactic extinction. However, this local dust should have no knowledge of the redshift distribution of the sources chosen.

On the other hand, in the case of lensing, the strength of the correlation depends on the efficiency with which the foreground lenses are able to magnify the distribution of background sources, as well as the observers ability to detect galaxies that are part of the lensing structure. Higher redshift sources are more efficiently lensed by higher redshift structures, which are composed of fainter galaxies. The measured correlation of high-redshift sources to foreground galaxies will be weaker in the lensing case because our galaxy sample has been chosen such that we are unable to detect these fainter galaxies.

We can confirm that there is no correlation between the redshift of the quasars with the $E(B-V)$ values obtained from the dust maps. In Figure 13, the quasar-galaxy angular correlation function is compared for three different distributions of the sources. Figure 13*a* shows the angular correlation function for the original set of 90 sources, whose redshift distribution is shown in Figure 2. For this source distribution, $0.7 < z < 2.9$, we have seen that the amplitude of the correlation function on scales of less than 5′ is 0.06 ± 0.02. This can be compared with $\omega_{QG}(\theta)$ in Figure 13*b*, where now the sample of 73 sources includes only those

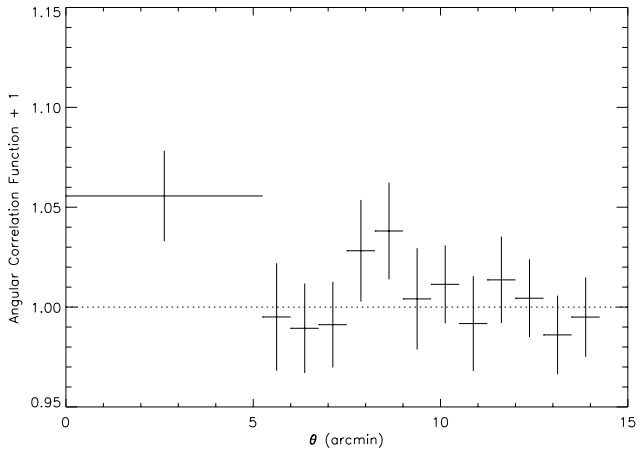


Fig. 13*a*

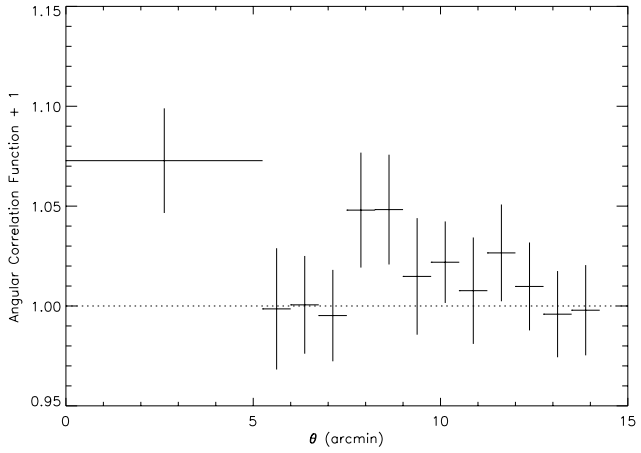


Fig. 13*b*

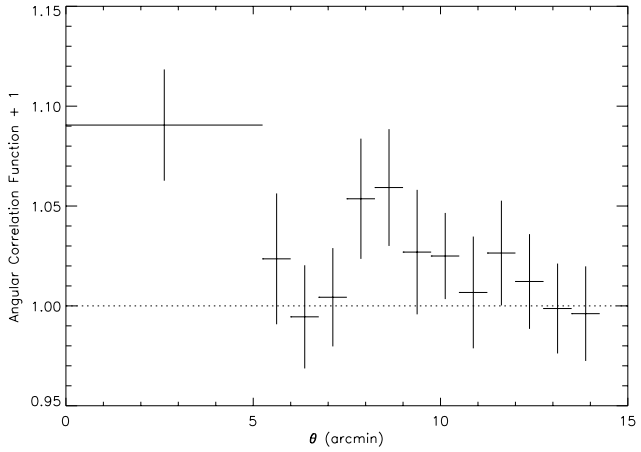


Fig. 13*c*

FIG. 13.—Correlation function for three different redshift distribution cuts of the data sample. (*a*) Original sample with all 90 quasars; (*b*) 73 quasars with redshifts $z < 2.0$; (*c*) 64 quasars with $z < 1.5$. As expected from gravitational lensing, the amplitude of the correlation increases as the quasar sample is restricted to redshifts in which the observed galaxies would be maximally efficient at lensing the sources.

quasars with redshifts of $z < 2.0$. The amplitude here is 0.07 ± 0.03. Figure 13*c* shows the same plot for a sample of 64 quasars with $0.7 < z < 1.5$ and an amplitude of 0.09 ± 0.03. The plots show that as the mean redshift of the

source sample decreases, the central amplitude of the correlation increases slightly without much increase in the rms error between the fields.

While the errors here are large, this trend is consistent with gravitational lensing as the explanation for these galaxy overdensities. As the distribution of source redshifts is decreased by discarding high-redshift quasars from the sample, the observed signal is strengthened. This is contrary to what is expected if intervening dust is the cause of the observed correlations.

For lensing, the signal is also expected to strengthen as the slope of the number density of the sources steepens. This can be achieved through a double magnification bias (Borgeest et al. 1991) by limiting the quasar sample appropriately. For example, limiting the optical magnitude of the quasars to magnitudes of less than 18.0 should steepen the slope of the number density function and increase the observed signal. Figure 14*a* shows a plot of $\omega_{QG}(\theta)$ for only bright quasars with optical magnitudes of less than 18.0. The amplitude of the correlation for these 45 fields is raised to 0.10 ± 0.04.

Similarly, limiting the sample to only those quasars with very bright radio fluxes should also artificially steepen the number density slope. For the 41 fields with quasars limited to be brighter than $S_{5\ \mathrm{GHz}} \geq 1.5$, the signal is increased to 0.11 ± 0.04, as shown in Figure 14*b*.

In this section, we have taken several cuts through the data sample in an attempt to evaluate the significance of dust obscuration to the observed correlation of galaxies and quasars. For each of these cuts, the resulting angular correlation function keeps with what is expected if the observed overdensities are due to gravitational lensing. This sample of radio quasars was initially selected so as to minimize the effects of dust on the results of our analysis. The arguments and plots presented above suggest that dust is not responsible for the signal observed in these fields.

6. DISCUSSION

The surface mass densities of clusters and large-scale structures containing galaxies at redshifts of 0.2–0.3 on scales of 0.8–1.0 h_{100}^{-1} Mpc are sufficient to cause the angular overdensities observed in this data set. However, as seen in our excess test, no rich clusters are observed in these data fields. This leaves poor clusters or diffuse large-scale structures as the likely lensing masses.

6.1. *Models of Quasar-Galaxy Correlations Due to Poor Clusters*

Croom & Shanks (1999) have compared a very simple lensing model with the observed underdensity of galaxies in the regions around UV-excess quasars of Boyle, Fong, & Shanks (1988). They model the lensing cluster as an isothermal sphere. They conclude that the required surface mass density needed to account for the observed anticorrelation suggests that the velocity dispersion, σ_v, of these lensing clusters is much larger than what is observed for poor clusters. They also include a simple lensing plane meant to simulate the effect of large-scale structures in addition to the isothermal sphere; however, they still find this model to be inconsistent with the amplitude of Boyle et al.'s measured correlation.

However, the much lower amplitude of the correlation observed with our data set is consistent with poor clusters as possible lensing mass structures for these quasars. Figure 15 shows the observed angular correlation function overplotted with the expectation for an isothermal sphere model (*dotted line*), assuming $\sigma_v = 400$ km s^{-1}, a cluster mass of $1.0 \times 10^{13}\ M_\odot$, and a lens redshift of $z = 0.22$. The other two models plotted include this isothermal sphere model, with an additional lens plane for large-scale structure in an Einstein–de Sitter universe (*dashed line*), and a Λ closed universe (*dot-dashed line*), with $\Omega_o = 0.3$, $\Lambda = 0.7$, and $H_0 = 50$ km s^{-1} Mpc^{-1}. This plot suggests that poor clusters may indeed be the lensing structures in the case of the correlations determined with this survey.

6.2. *Semianalytic Models of Quasar-Galaxy Correlations Due to Large-Scale Structure*

Detailed simulations of light propagation in a clumpy universe have been performed by DB97 and Sanz et al. (1997), for various cosmological parameters, with the express purpose of simulating the background quasar–foreground galaxy angular correlation function. Essentially,

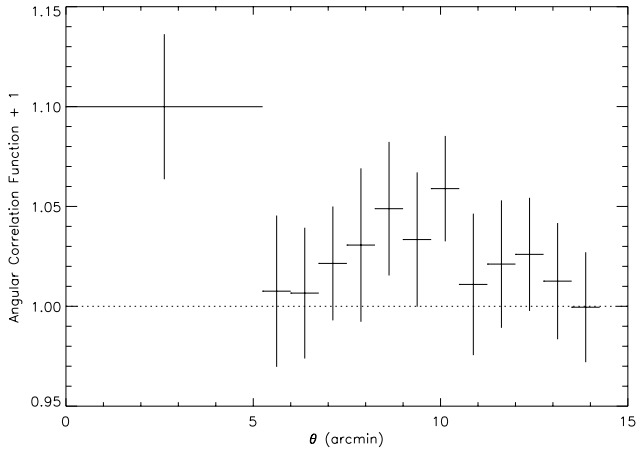


Fig. 14*a*

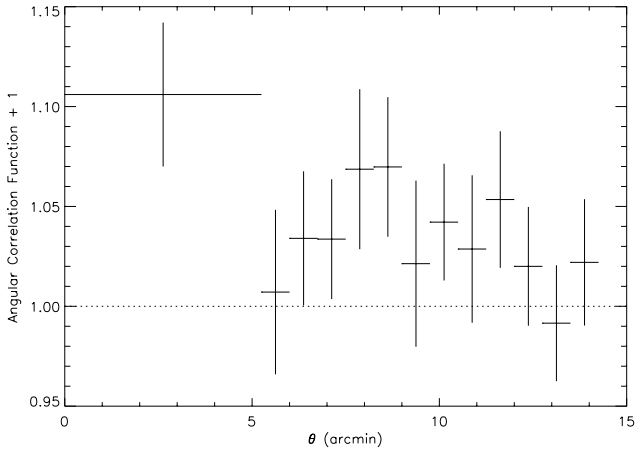


Fig. 14*b*

FIG. 14.—Correlation function plotted for two different cuts of the source sample, designed to increase the magnification bias signal. (*a*) The quasar sample has been restricted to quasars with optical magnitudes brighter than 18.0. The amplitude of the signal is increased in keeping with what is expected from gravitational lensing models, if multiple magnification bias is significant. (*b*) This quasar sample includes only sources with radio fluxes of greater than 1.5 Jy. Again, the signal is increased slightly by restricting the sample to apparently brighter objects.

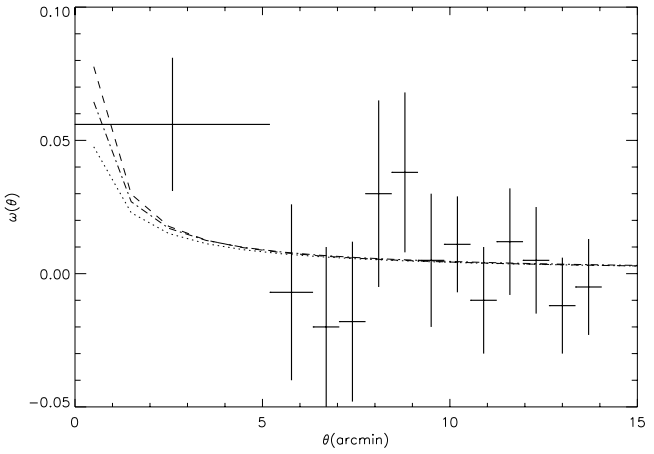


FIG. 15.—Observed angular correlation function for 90 quasar fields overplotted with models of lensing by a poor cluster, represented by an isothermal sphere model. The dashed line shows the model with an isothermal sphere, with $\sigma_v = 400$ km s^{-1} and a mass of $1 \times 10^{13}\ M_\odot$, as the lensing structure. The other two models include a planar component, intended to represent (in a simple way) additional lensing due to large-scale structures. The dashed line shows an Einstein–de Sitter model, while the dot-dashed line shows a $\Omega_o = 0.3, \Lambda = 0.7, H_0 = 50$ km s^{-1} Mpc^{-1} model.

both groups use the same method and attain similar results. DB97 have very graciously allowed us access to their Fortran code in order to compare their models specifically with this quasar sample.

The method used in DB97 is an extension of the work done by B95. In his paper, B95 shows that the quasar-galaxy correlation function can be written as

$$\omega_{\rm QG}(\theta) = (\alpha - 1) b \omega_{\mu\delta}(\theta)\ . \qquad (2)$$

The quantities α and b are the slope of the cumulative number density function of the sources and the bias, respectively. The quantity $\omega_{\mu\delta}(\theta)$ is the correlation between the magnification, μ, and density contrast, δ, as a function of the angular scale. We define the magnification as the brightening of the background sources due to enhancement by gravitational lensing. This lensing is induced by density contrasts encountered along the line of sight to the observer. These density contrasts (mass fluctuations) are dependent on cosmological parameters that lead to differences in large-scale structure formation on various angular scales. In particular, along with specifications for Ω_0, Λ, and H_0, models must specify the type of dark matter, the initial power spectrum of mass fluctuations, and the evolution of this power spectrum.

We have run the models of DB97 with the redshift distribution of quasars used here (see Fig. 2) for a variety of cosmological models. All the models shown include nonlinear evolution of the matter power spectrum and are calculated for cold dark matter (CDM). For each model, Ω_0, Λ, and H_0 are specified, as well as the normalization of the power spectrum through the parameter σ_8 (the rms density variation of galaxies over an $8\ h_{100}^{-1}$ Mpc sphere).

Figure 16*a* shows the quasar-galaxy angular correlation function, determined from this survey, overplotted with the CDM models for four different choices of cosmological parameters. For these plots, the central region around the quasar has been partitioned into annuli with widths of 0.′75. The models calculate $\omega_{\mu\delta}(\theta)$, therefore the curves plotted in the figures have been scaled by $(\alpha - 1)$ and a bias of $b = 1/\sigma_8$.

Figure 16*b* shows our doubly limited quasar sample, i.e., only quasars with optical magnitudes of less than 18 are used, overplotted with the same models; however, now $\alpha = 3$.

The scale of the overdensity does appear to match the scale seen in the models, that is, the models show the scale of the overdensity to be $\lesssim 5'$. The amplitude of the observed correlation on scales of $\sim 1.'5$–$2'$ is generally consistent with the models; however, the errors on the data are too large to distinguish between the different cosmologies.

Figures 16*a* and 16*b* show the consequences of varying cosmological parameters on the amplitude and shape of the angular correlation function. In general, high Hubble constant models have larger correlation amplitudes than low H_0 models; this is seen by comparing the $H_0 = 50$ km s^{-1} Mpc^{-1} open model (*dot-dashed line*) with the $H_0 = 100$ km s^{-1} Mpc^{-1} open model (*dotted line*). Simply, this is because the peak in the power spectrum shifts to larger wavenum-

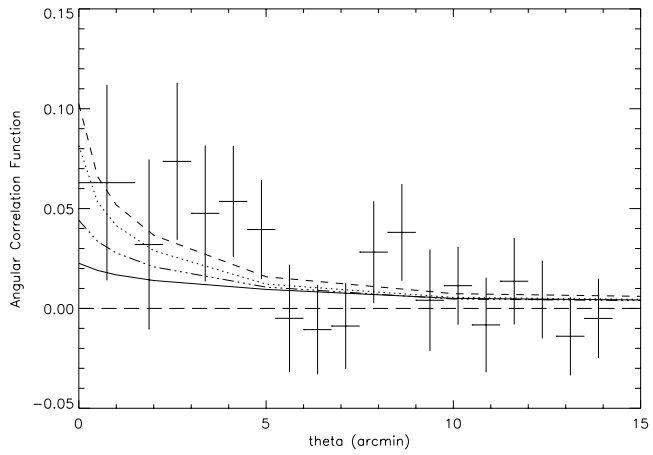


Fig. 16*a*

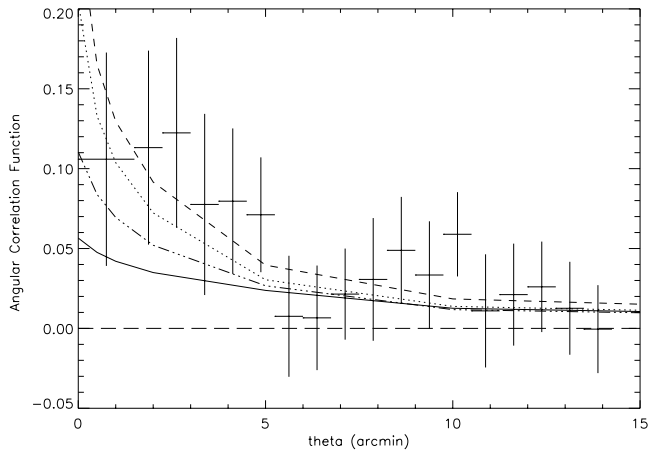


Fig. 16*b*

FIG. 16.—Observed angular correlation function overplotted with CDM models of DB97. (*a*) For the total quasar distribution used in this survey, the models have been scaled by $\alpha - 1 = 0.8$ and $b = 1/\sigma_8$. (*b*) The angular correlation function overplotted with CDM models of DB97 for the doubly limited quasar distribution (optical magnitude is <18). Models have been scaled by $\alpha - 1 = 2$ and $b = 1/\sigma_8$. Cosmological parameters for each model are as follows: (*solid line*) $H_0 = 50, \Omega_m = 0.3, \Omega_\Lambda = 0.7, b =$ cluster biasing; (*dot-dashed line*) $H_0 = 50, \Omega_m = 0.3, \Omega_\Lambda = 0, b =$ cluster biasing; (*dotted line*) $H_0 = 100, \Omega_m = 0.3, \Omega_\Lambda = 0, b =$ cluster biasing; (*dashed line*) $H_0 = 100, \Omega_m = 0.3, \Omega_\Lambda = 0, b = 1.0$ biasing. Note that the dashed-line model shows a flatter profile.

bers (smaller scales) as H_0 increases. This boosts the density fluctuations on small scales, which leads to higher magnifications on those scales. Open models (*dot-dashed line*) have larger amplitudes than closed Λ models (*solid line*). The explanation for this is that Λ models have more growth of density perturbations. Therefore, in these models, there is more power on large scales than for open models. Open models, with relatively more power on small scales, will show a larger amplitude of the correlation function.

A change in the normalization parameter, σ_8, also has an effect on the amplitude of the correlation function at small and large scales. A comparison of the dotted and dashed lines shows the effect of going from a cluster normalization to $\sigma_8 = 1$. For the cluster-normalized model, σ_8 is determined by counting the number of clusters; in particular, we use the findings of Eke, Cole, & Frenk (1996), in which they find $\sigma_8 = 0.5\Omega_o^{-0.47+.1\Omega_o}$ for a $\Lambda = 0$ universe. For a value of $\Omega_o = 0.3$, this gives $\sigma_8 = 0.85$. As expected, the amplitude of the model with $\sigma_8 = 1$ is larger.

This comparison of the angular correlation function measured here and the CDM models of DB97 gives additional evidence that the quasars in these fields are being magnified primarily by large-scale structures. The fact that the models and data agree down to small angular scales suggests that there is very little contribution to the lensing observed here from compact objects. The scale ($\sim 5'$) of the lensing also agrees with the models and further suggests that the structures responsible are located at $z = 0.2$–0.3, and thus these structures have physical sizes of $\gtrsim 0.6\, h_{100}^{-1}$ Mpc.

This initial result suggests that cosmologically meaningful surveys can be carried out on small telescopes equipped with wide-field imagers. The detection of magnification bias and statistical gravitational lensing is a strong confirmation of the current paradigm of gravity and large-scale structure formation. Figure 16 suggests that galaxy sample sizes 8–10 times larger than employed in this survey can discriminate between cosmological models.

This will not be easy to achieve. Deeper imaging with better star-galaxy separation could increase the sample size of galaxies in each field, but at some point the surveys would begin to pick up dwarf galaxies at the lens redshifts, along with many more luminous galaxies at higher redshifts. An increase in the size of the source sample by any large factor could thus weaken the magnification bias signal. The most promising strategy is to use photometric redshifts to exert selection against background galaxies, thereby increasing the sensitivity of the experiment.

The authors would like to thank C. Petry for obtaining the 90 inch data. In addition, special thanks to K. Dolag and M. Bartelmann for providing their models. Thanks also to the reviewer for the useful comments. This research made use of the NASA/IPAC Extragalactic Database (NED), which is operated by the Jet Propulsion Labortory, California Institute of Technology, under contract with the NASA. The Digitized Sky Surveys were produced at the Space Telescope Science Insitute under US government grant NAG W-2166. D. J. N. would like to acknowledge support from NASA GSRP S96-UMF-003 and the Danforth-Compton Fellowship. C. D. I. acknowledges NSF support from award AST 98-03072.

REFERENCES

Abraham, R., et al. 1996, ApJ, 471, 694
Bartelmann, M. 1995, A&A, 298, 661 (B95)
Bartelmann, M., & Schneider, P. 1991, A&A, 248, 349
———. 1993a, A&A, 268, 1
———. 1993b, A&A, 271, 421
———. 1994, A&A, 284, 1
Bartsch, A., Schneider, P., & Bartelmann, M. 1997, A&A, 319, 375
Benítez, N., & Martínez-González, E. 1995, ApJ, 448, L89
———. 1997, ApJ, 477, 27
Borgeest, U., von Linde, J., & Refsdal, S. 1991, A&A, 251, L35
Boyle, B. J., Fong, R., & Shanks, T. 1988, MNRAS, 231, 897
Broadhurst, T., Ellis, R., & Shanks, T. 1988, MNRAS, 235, 827
Canizares, C. 1981, Nature, 291, 620
Colless, M., Ellis, R., Broadhurst, T., Taylor, K., & Peterson, B. 1993, MNRAS, 261, 19
Croom, S. M., & Shanks, T. 1999, MNRAS, 307, L17
Dolag, K., & Bartelmann, M. 1997, MNRAS, 291, 446 (DB97)
Eke, V., Cole, S., & Frenk, C. 1996, MNRAS, 282, 263
Kendall, M., & Stuart, A. 1973, The Advanced Theory of Statistics, Vol. 2 (London: C. Griffin)
Kühr, H., Witzel, A., Pauliny-Toth, I., & Nauber, U. 1981, A&AS, 45, 367
Landolt, A. 1992, AJ, 104, 340
Maddox, S., Efstathiou, G., & Sutherland, W. 1996, MNRAS, 283, 1227
Metcalfe, N., Shanks, T., Fong, R., & Jones, L. 1991, MNRAS, 249, 498 (MSFJ)
Norman, D., & Impey, C. D. 1999, AJ, 118, 613 (Paper I)
Norman, D., & Williams, L. L. R. 2000, AJ, 119, 2060
Press, W., Teukolsky, S., Vetterling, W., & Flannery, B., 1986, Numerical Recipes in Fortran (Cambridge: Cambridge Univ. Press)
Sanz, J., Martínez-González, E., & Benítez, N. 1997, MNRAS, 291, 418
Schlegel, D., Finkbeiner, D. J., & Davis, M. 1998, ApJ, 500, 525
Schneider, P., Ehlers, J., & Falco, E. 1992, Gravitational Lenses (New York: Springer)
Stickel, M., Meisenheimer, K., & Kühr, H. 1994, A&AS, 105, 211
Tody, D. 1986, Proc. SPIE, 627, 733
Tyson, J. 1986, AJ, 92, 691
Williams, L., & Irwin, M. 1998, MNRAS, 298, 378
Wu, X., & Fang, L. 1996, ApJ, 461, L5